JGR Oceans

RESEARCH ARTICLE
10.1029/2023JC020568

Primary Production and Respiration in the Norwegian Sea Estimated From Biogeochemical Argo Floats

Kjell Arne Mork[1], Kjell Gundersen[1], Knut Yngve Børsheim[1], Giorgio Dall'Olmo[2], Øystein Skagseth[1], and Henrik Søiland[1]

[1]Institute of Marine Research and the Bjerknes Centre for Climate Research, Bergen, Norway, [2]National Institute of Oceanography and Applied Geophysics – OGS, Sgonico, Italy

Key Points:

- Seasonal and annual biological production were quantified for 2020 and 2021, utilizing two biogeochemical Argo floats in the Norwegian Sea
- Cold wind in April 2021 caused slower bloom progression and nitrate consumption, resulting in reduced phytoplankton biomass compared to 2020
- Vertical nitrate flux due to physical mixing doubled the net community production (NCP) during the seasonal growth period for both years

Supporting Information:

Supporting Information may be found in the online version of this article.

Correspondence to:

K. A. Mork,
kjell.arne.mork@hi.no

Citation:

Mork, K. A., Gundersen, K., Børsheim, K. Y., Dall'Olmo, G., Skagseth, Ø., & Søiland, H. (2024). Primary production and respiration in the Norwegian Sea estimated from biogeochemical Argo floats. *Journal of Geophysical Research: Oceans*, *129*, e2023JC020568. https://doi.org/10.1029/2023JC020568

Received 12 OCT 2023
Accepted 31 MAY 2024

Author Contributions:

Conceptualization: Kjell Arne Mork
Methodology: Kjell Arne Mork, Kjell Gundersen, Knut Yngve Børsheim, Giorgio Dall'Olmo, Øystein Skagseth, Henrik Søiland
Writing – original draft: Kjell Arne Mork, Kjell Gundersen, Knut Yngve Børsheim, Giorgio Dall'Olmo, Øystein Skagseth, Henrik Søiland
Writing – review & editing: Kjell Arne Mork, Kjell Gundersen, Knut Yngve Børsheim, Giorgio Dall'Olmo, Øystein Skagseth, Henrik Søiland

Abstract Biogeochemical (BGC) Argo floats were used in this study to investigate phytoplankton blooms. We assessed the seasonal and annual rates of net primary and community production, along with respiration in the Norwegian Sea. The years 2020 and 2021 were contrasted to illuminate similarities and differences. In both years the onset of the bloom occurred at the beginning of February, coinciding with a deep winter mixed layer. However, during spring and summer the biological production appeared to develop differently. In 2020 the mixed layer depth shoaled quickly in April due to surface heating, triggering a strong spring bloom event. In contrast, a significant surface cooling in April 2021 triggered a substantial vertical mixing, that delayed the mixed layer's shoaling. This delay initiated cascading effects impacting nitrate consumption and bloom development that resulted in increased respiration in 2021 compared to 2020. In both years, vertical nitrate mixing from deeper layers to the surface emerged as a pivotal factor determining primary production. Using a mixed layer model in combination with Argo observations, we found that the upward nutrient fluxes due to mixing doubled net community production. These findings underscore the capability of BGC-Argo floats, operating at a 5-day resolution, to unveil the intricate interplay between hydrography, physical drivers, and biogeochemical processes in shaping phytoplankton dynamics and overall ecosystem productivity in the Norwegian Sea.

Plain Language Summary The magnitude of seasonal phytoplankton growth is complex but generally depends on several physical and chemical variables. Thus, estimating the annual phytoplankton production accurately is a challenging task as it requires measurements with high temporal resolution over a full season. In this study, we used data from two vertical biogeochemical profiling Argo floats, operating at 5 days resolution. Combined with a mixed layer model, we resolved the development of phytoplankton production and respiration in the Norwegian Sea. We found that the vertical mixing of nutrients from deeper layers to the surface appeared as a determining factor on phytoplankton production and contributed to 50% of the production. In 2021, an anomalous wind and cooling event in April caused deep mixing at the onset of the spring bloom. This caused a slower and delayed phytoplankton growth and nutrient consumption, resulting in higher grazing of phytoplankton and reduced phytoplankton biomass, compared to the 2020 spring bloom. This study demonstrates the unique capability of Argo floats to resolve coupled physical-biogeochemical processes including phytoplankton growth dynamics in the Norwegian Sea.

1. Introduction

Hydrographic conditions in the upper layer of the southern Norwegian Sea, the Norwegian Basin, are influenced by two main water masses. Warm and saline Atlantic Water (AW) is flowing northward on the eastern side of the basin, and the relative less saline and colder Arctic waters are transported into the area from the west (Helland-Hansen & Nansen, 1909; Figure 1). The upper layers in the central Norwegian Basin are therefore occupied by modified AW, which is a mixture of these two water masses. Below the upper layers and above the deep water lies the Arctic Intermediate Water, that originates from the Greenland and Iceland Seas as a product of winter convection (Blindheim, 1990; Jeansson et al., 2017).

The Norwegian Sea is a highly productive area with a pronounced seasonal cycle in terms of light, temperature and dissolved nutrients driving primary production (Skjoldal, 2004). In winter, intense surface cooling and strong winds deepen the mixed layer depth (MLD) to several hundred meters (Nilsen & Falck, 2006). Winter mixing events bring nutrient-rich deep water to the surface creating an even distribution of nutrients throughout the winter mixed layer. The magnitude of the seasonal phytoplankton bloom is determined by the amount of nutrients

Table 1
Argo Float Information

Float ID	Abbreviation	Cycle time	Calendar year	First profile	Last profile	Float model
6903549	A	5 days	2020	05 Jan 2020	30 Dec 2020	PROVOR CTS4
6903574	B	5 days	2021	03 Jan 2021	29 Dec 2021	PROVOR CTS4

renewed from deep waters during winter mixing (e.g., Rey, 2004; Sundby et al., 2016). Skagseth et al. (2022) described the hydrography and seasonal nutrient dynamics in the Norwegian Basin for the period 1995–2019, and from 2017, a "freshening" of the Atlantic layer was observed due to expansion of low saline Arctic water with higher nitrate and silicate content.

The magnitude of seasonal phytoplankton growth is complex and depends on several physical and chemical parameters (e.g., Rey, 2004). Until more recently, we were not able to estimate these parameters with great accuracy, as annual primary production estimates require sampling at high frequency to resolve the considerable temporal variabilities of the processes (Rey, 2004). In recent years, however, biogeochemical (BGC) Argo profiling floats operating at high temporal resolution have been providing persistent observations on seasonal to interannual scales and have successfully been used to study phytoplankton blooms, respiration and carbon export (e.g., Briggs et al., 2018; Bushinsky & Emerson, 2018; Dall'Olmo & Mork, 2014; Johnson et al., 2017; Plant et al., 2016; Yang et al., 2021). Here we present the first investigation of annual net primary and community production, including respiration in the Norwegian Sea using BGC-Argo data.

Net Community Production (NCP) is the difference between gross primary production (GPP) and community respiration (heterotrophic and autotrophic respiration of photosynthetic products). Dugdale and Goering (1967) defined the primary production based upon nitrate brought into the euphotic zone by winter mixing as new production. Williams (1993) equated new production to NCP only on annual scales, defining NCP as the upper limit for annual carbon export from surface waters (Brix et al., 2006; Emerson, 1987). In the Norwegian Sea estimates of NCP were often derived from annual budgets of nitrate or oxygen concentrations (e.g., Falck & Anderson, 2005; Skjelvan et al., 2001) or from settling rates of particulate carbon (Wassman, 1990). The contribution of autotrophic respiration has traditionally been associated with a large uncertainty due to lack of direct measurements, for example, by the Winkler bottle incubation method. However, Yang et al. (2021) used recent BGC Argo-profiles in the North Atlantic to estimate net primary production (NPP), the difference between GPP and only autotrophic respiration, using chlorophyll-a content and optical backscattering measurements.

In this study, we used data from two BGC-Argo floats in the Norwegian Basin to quantify the annual cycle of phytoplankton. We estimated seasonal and annual rates of NPP, NCP, and respiration over the years 2020–2021. Annual NCP was estimated from nitrate consumption assuming a fixed carbon:nitrogen relationship (Redfield et al., 1963). We contrasted the 2 years to demonstrate similarities and differences of the responses of growth dynamics and biogeochemistry with respect to hydrography and physical forcing. Specifically, we investigated the influence of physical mechanisms, particularly vertical mixing, on bloom development, nitrate consumption, NCP, and respiration.

2. Methods

2.1. Biogeochemical Argo Floats

Two BGC-Argo floats were deployed sequentially in the Norwegian Basin, first in May 2019 and then in August 2020, respectively (Table 1). When appropriate, abbreviation of the floats is hereafter described as A (float 6903549) and B (float 6903574), respectively.

In March 2021, float A drifted out of the Norwegian Basin and into the Lofoten Basin. As the hydrographic conditions are different for these two basins, only data from year 2020 were used for this float. Float B drifted counterclockwise in the Norwegian Basin the whole lifetime and data from its first calendar year (2021) were used in this study as a comparison with year 2020. All the time series and budget values for the years 2020 and 2021 are therefore based on data from floats A and B, respectively (Table 1). The trajectories of the floats within each calendar year are shown in Figure 1. The floats were programmed to have a parking depth at 1,000 dbar and to profile from 2000 dbar to surface every 5 days. Both floats were equipped with a Conductivity, Temperature,

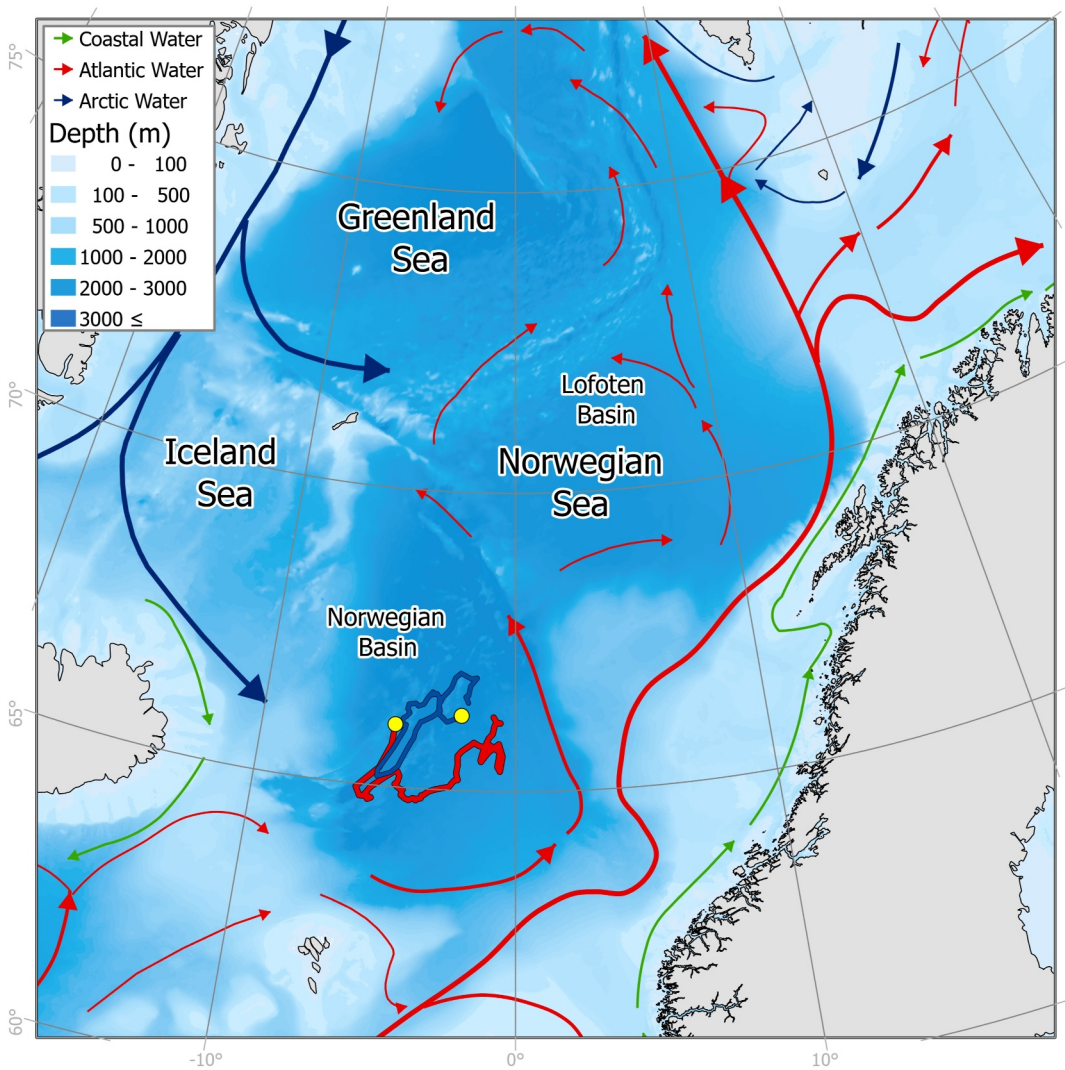

Figure 1. Schematic view of the main surface currents in the Nordic Seas and the tracking of float A (red line) and B (blue line) during 2020 and 2021, respectively. Yellow dot indicates location of the first profile within each calendar year. Color contours represent the bottom depths (upper left corner).

Depth (CTD) instrument, together with nitrate, chlorophyll a (Chl-*a*) and optical backscatter (b_{bp}) sensors, and a photosynthetically available radiation (PAR) sensor. The details of the sensors are given in Table 2.

The Argo data were downloaded from the Coriolis Data Center (France) after quality control as recommended by the international Argo Data Management Team (ADMT, Bittig et al., 2019). The Chl-*a* data were corrected for an

Table 2
Sensor Information

Variable	Sensor
CTD	Seabird 41CP
Nitrate	Submersible ultraviolet nitrate analyzers (SUNA) optical sensor from Satlantic
Chl-*a* and b_{bp}	Seabird ECO triplet with a fluorometer and a backscattering sensor at 700 nm
PAR	OCR-504 radiometer from Satlantic measuring downwelling irradiance integrated over 400–700 nm

in-situ instrument dark signal, non-photochemical quenching (Schmechtig et al., 2018), and divided by a factor 2 to account for a calibration error in fluorometers (Roesler et al., 2017) as recommended by ADMT. The backscatter data (b_{bp}) were calculated from the sensor output using the manufacturer's coefficients, and quality controlled (range and spike tests) in real time at Coriolis Data Center. Additionally, all data were checked visually before use. The Chl-*a* profiles, together with profiles of b_{bp}, were used to compute particulate organic carbon (POC) using the algorithm from Koestner et al. (2022).

$$POC^{*} = k_1 \cdot b_{bp}{}^{k_2} \cdot r^{k_3} \cdot r^{k_4 \log b_{bp}} \tag{1}$$

$$POC = \begin{cases} \varepsilon_1 \cdot POC^{*} - \varepsilon_2, & POC^{*} < POC_{min} \\ POC^{*}, & POC^{*} \geq POC_{min} \end{cases} \tag{2}$$

where r is the ratio $r = \text{Chl-}a/b_{bp}$ and the coefficients (k_1, k_2, k_3, k_4, ε_1, ε_2) and POC_{min} are given by Koestner et al. (2022). The drift and bias in the nitrate data were corrected by comparing the data at 2000 m depth with World Ocean Atlas 2018 (Garcia et al., 2018), and applying the calculated anomaly at depth to the entire profile. Eventually, the corrected data were validated with nitrate measurements from *in-situ* water samples collected during each deployment of the Argo floats.

The MLD was defined as the depth where the difference between potential density at depth and at 10 m equals 0.03 kg m^{-3} (e.g., de Boyer Montégut et al., 2004; Holte et al., 2017). We assume 0.415 mol quanta m^{-2} day^{-1} to be the threshold depth (z_{PAR}) where the depth below was insufficient to support photosynthesis (Boss & Behrenfeld, 2010; Letelier et al., 2004). By using BGC-Argo data in the Southern Ocean, Arteaga et al. (2022) showed that 90% of total NPP in a vertical profile was within the 0-z_{PAR} layer. Depth integration of Chl-*a*, POC, NPP and NCP were calculated for each profile and over the depths where the vertical profile of annual NCP was positive (see Plant et al., 2016 for details). For the Norwegian Basin, NCP stayed positive between surface and 42 m depth for both years (see Results).

2.2. Net Primary Production

Net primary production (NPP) was estimated from the carbon-based productivity model (CbPM), originally from Westberry et al. (2008), that was modified for use with BGC-Argo floats to estimate vertical profiles of NPP (Arteaga et al., 2022). NPP is the product of phytoplankton carbon and phytoplankton growth rate:

$$NPP = \mu \cdot C_{phyto} \tag{3}$$

where C_{phyto} is phytoplankton carbon and μ is phytoplankton growth rate. C_{phyto} estimates are obtained from the Argo b_{bp} profiles using the empirical relationship (Graff et al., 2015):

$$C_{phyto} = 12128 \cdot b_{bp}(470) + 0.59 \tag{4}$$

where b_{bp} at 470 nm is estimated from b_{bp} at 700 nm (Morel & Maritorena, 2001):

$$b_{bp}(470) = \frac{700}{470} \cdot b_{bp}(700) \tag{5}$$

For each $b_{bp}(700)$ profile spikes were removed using a median filter. The averaged concentration between 1900 and 2000 m was subtracted from the entire vertical profile in advance of the calculation to ensure that phytoplankton carbon approaches zero at depth (Arteaga et al., 2020).

The phytoplankton growth rate μ at each depth in Equation 3 is a function of the maximum growth rate ($\mu_{max} = 2$ $days^{-1}$, Banse, 1991), light limitation index I_{light} and the cellular nutrient index I_{nut}:

$$\mu = \mu_{max} \cdot I_{light} \cdot I_{nut} \tag{6}$$

The light index (I_{light}) is a function of the local light level (PAR) at each depth while the nutrient stress index (I_{nut}) is a function of the Chl-*a*:C_{phyto} ratio and PAR (Behrenfeld et al., 2005; Westberry et al., 2008). Both light and

nutrient indices range from 0 to 1. The Argo floats used by Arteaga et al. (2022) were not equipped with *in-situ* light sensors, so they used satellite PAR data from sea surface that were depth resolved using the diffuse attenuation coefficient derived from Chl-*a* concentrations. In this study, both Argo floats were equipped with light sensors. The floats were programmed to surface at noon to record maximum light levels. A daily light profile was estimated by combining the float PAR measurement at noon with the theoretical solar elevation and day length as function of the float's location and day of year (e.g., Berger, 1978).

2.3. Net Community Production

Net community production (NCP) of organic carbon was estimated as the net biological consumption of nitrate. New (nitrate) production (Dugdale & Goering, 1967) only approaches NCP on annual scales (Williams, 1993). Therefore, on seasonal and longer time scales, we assume new production to be equivalent to NCP in this study (Platt et al., 1989; Williams, 1993). Since the change in nitrate concentrations with depth is a sum of both physical (mixing and advection) and biological (incorporation) processes, they were separated:

$$\left(\frac{\partial N}{\partial t}\right)_{observed} = \left(\frac{\partial N}{\partial t}\right)_{biology} + \left(\frac{\partial N}{\partial t}\right)_{physics} \quad (7)$$

A one-dimensional mixed layer model (PWP-model, Price et al., 1986) was used to estimate the physical signal of changes in nitrate concentrations, as suggested by Plant et al. (2016). The PWP-model was initialized with a depth profile of temperature, salinity and nitrate, and run until the next float profile. The difference in nitrate (N) between observations (float data) and the model results determined at time n + 1 (t_{n+1}) was interpreted to be the biological component:

$$\left(\frac{\partial N}{\partial t}\right)_{biology} = \frac{N_{observed}(t_{n+1}) - N_{model}(t_{n+1})}{t_{n+1} - t_n} \quad (8)$$

The physical signal was determined by the difference between the model results at time t_{n+1} and the initialized float profile at time t_n:

$$\left(\frac{\partial N}{\partial t}\right)_{physics} = \frac{N_{model}(t_{n+1}) - N_{observed}(t_n)}{t_{n+1} - t_n} \quad (9)$$

The profile of biological incorporation of nitrate rate in Equation 8 was converted to carbon (C) and NCP using the Redfield C:N-ratio of 106:16 (Redfield et al., 1963). Positive or negative NCP imply net production or net respiration rates, respectively. Averaged annual NPP and NCP were calculated for the years 2020 (float A) and 2021 (float B), as depth integrations over the time-course of each calendar year.

In the PWP-model it is assumed that the horizontal flux of nitrate is negligible compared to the vertical fluxes (e.g., Gislefoss et al., 1998). This assumption looks also justified since the strongest currents are at the rim of the Norwegian Basin, while currents appear weaker in the interior (Søiland et al., 2008; Voet et al., 2010) where the two BGC-Argo floats drifted (Figure 1). Previous estimates of annual NCP in the Norwegian Sea have also been based on this assumption (e.g., Falck & Anderson, 2005; Possenti et al., 2021; Skjelvan et al., 2001).

2.4. Optimizing the Mixed-Layer Model

The PWP-model (Price et al., 1986) was forced by air-sea heat and freshwater fluxes and wind, using the ERA5 reanalysis data set with one-hourly temporal resolution (Hersbach et al., 2020). The model was initialized with Argo temperature and salinity depth profiles that were interpolated onto the model grid with 1-m vertical resolution. At each model time step, 1 hr in our case, the model checked for internal stabilities, and performed mixing with depth to remove instabilities. Following Glover et al. (2011) the model was optimized to reproduce local physical condition as best as possible (details in Text S1 in Supporting Information S1). There are three parameters in the model that can be tuned. These include the vertical mixing coefficient and offsets of heat and freshwater fluxes, that can be derived, for example, from errors in the air-sea heat and freshwater fluxes and horizontal advection that are not included in the model. During the optimization, the model was run freely for

1 year several times over with a range of different values for the vertical mixing coefficient and offsets of heat and freshwater fluxes. Modeled surface temperature and salinity, including the MLD, was compared with the observations for all runs that gave an optimized vertical mixing coefficient about 10^{-4} $m^2 s^{-1}$ (Figure S1 in Supporting Information S1). In the Nordic Seas, the mixing coefficient in the upper layer has been estimated to be in the range of 10^{-5}–10^{-4} m^2 s^{-1}, depending on the level of stratification (Naveira Garabato et al., 2004). Thus, our value is in the upper range. Furthermore, 12 W m^{-2} of heat for both 2020 and 2021 (Figure S1 in Supporting Information S1) was added to the surface in addition to the ERA5 air-heat sea heat fluxes. The added heat flux likely accounted for horizontal advection of heat from AW into the basin. These offsets were small compared to the air-sea heat fluxes that ranged from ∼−400 W m^{-2} to ∼200 W m^{-2}. No additional freshwater flux was needed to optimize the model.

The modeled surface temperature and salinity, including MLD, agreed well with the observations when the model was run freely over 1 year with the optimized values. During the last four months, modeled surface temperature was too high in 2020 and too low in 2021 (Figure S2 in Supporting Information S1). The modeled MLD agreed well with the observed MLD in 2020 but in 2021 the model overestimated the MLD during winter (Figure S2 in Supporting Information S1). Even so, the model appeared to reflect the physical conditions quite well.

After the model was optimized, it was run for the whole period for each float and initialized every fifth day. The observed data showed evidence of internal waves (see Figure 2) that the PWP-model could not simulate. This resulted in unrealistic temporal oscillations in the nitrate rates and NCPs near the base of the mixed layer. In order to correct for this discrepancy, Plant et al. (2016) stretched or compressed the water column above and below the modeled MLD to match the observed MLD from float data. However, this introduced new errors around the MLD. To overcome this mismatch, Briggs et al. (2018) integrated the NCP to a depth shallower than the MLD. Instead, we filtered the depth-integrated NCP series in time using a low pass seven-point Hamming filter, to remove oscillations with periods less than 1 month in order to maintain monthly resolution.

3. Results

3.1. Biogeochemical Argo Data

Seasonal temperature, salinity, nitrate concentrations, backscatter, and Chl-*a* in the upper 400 m together with the MLD and z_{PAR} during 2020 and 2021 are shown in Figure 2. The MLD reached a maximum at 248 m (2020) and 226 m (2021) depth during winter and a seasonal minimum at 15 m in summer for both years. The MLD in 2020 decreased from 200 m to less than 50 m during April, while it took approximately two months in 2021 (April–May) to reach the same seasonal minimum. In winter and early spring (January–April) the water column above the MLD was homogenous with temperatures of about 4°C, and during seasonal heating surface temperatures were higher than 10°C in summer for both years. Both years had maximum nitrate concentrations in the mixed layer above 10 μmol kg^{-1} during winter. Below the mixed layer, nitrate concentrations were higher and the mixing during winter therefore determined the mixed-layer nitrate concentrations. Concurrently with the development of a shallow MLD in both years, we observed a rapid drawdown of nitrate in the mixed layer due to biological production. During autumn and winter, nitrate concentrations increased as deeper mixing brought nutrient-rich deep water into to surface waters. Surface backscatter data peaked during the May–June transition in both years, but the peak was more pronounced in 2020. In 2021 however, higher particle concentrations were observed at greater depths. Sinking of particles below the mixed layer were observed for both years during spring and summer.

Minimal Chl-*a* concentrations (0.01 mg m^{-3}) appeared in general at depths similar to MLD, in spring and prior to the seasonal (Figure 2). The low Chl-*a* concentrations observed during winter (>0.01 mg m^{-3}), for both years, indicated net growth of phytoplankton even during deep winter mixing. Toward the second half of January (2020) and mid-February (2021), the modeled mixing depth was frequently shallower than the light level, z_{PAR}. Thus, vertical active mixing of the water column at that time meant that the phytoplankton, periodically, remained within the photic zone. As a result, accumulation of Chl-*a* already started at the beginning of February for both years (Figure 2, Chl-*a*). Phytoplankton growth continued through summer into November for both years, at which time the mixed layer deepened and surface light levels decreased. Maximum z_{PAR} appeared in spring (March–April) and approximately at 80 m depth for both years. At the start of the spring bloom period, we observed a shoaling of z_{PAR} due to an increase in light attenuation caused by increasing numbers of more suspended particles at surface (see Figure 2, b_{bp}). However, z_{PAR} was in general located deeper than the MLD during summer for both

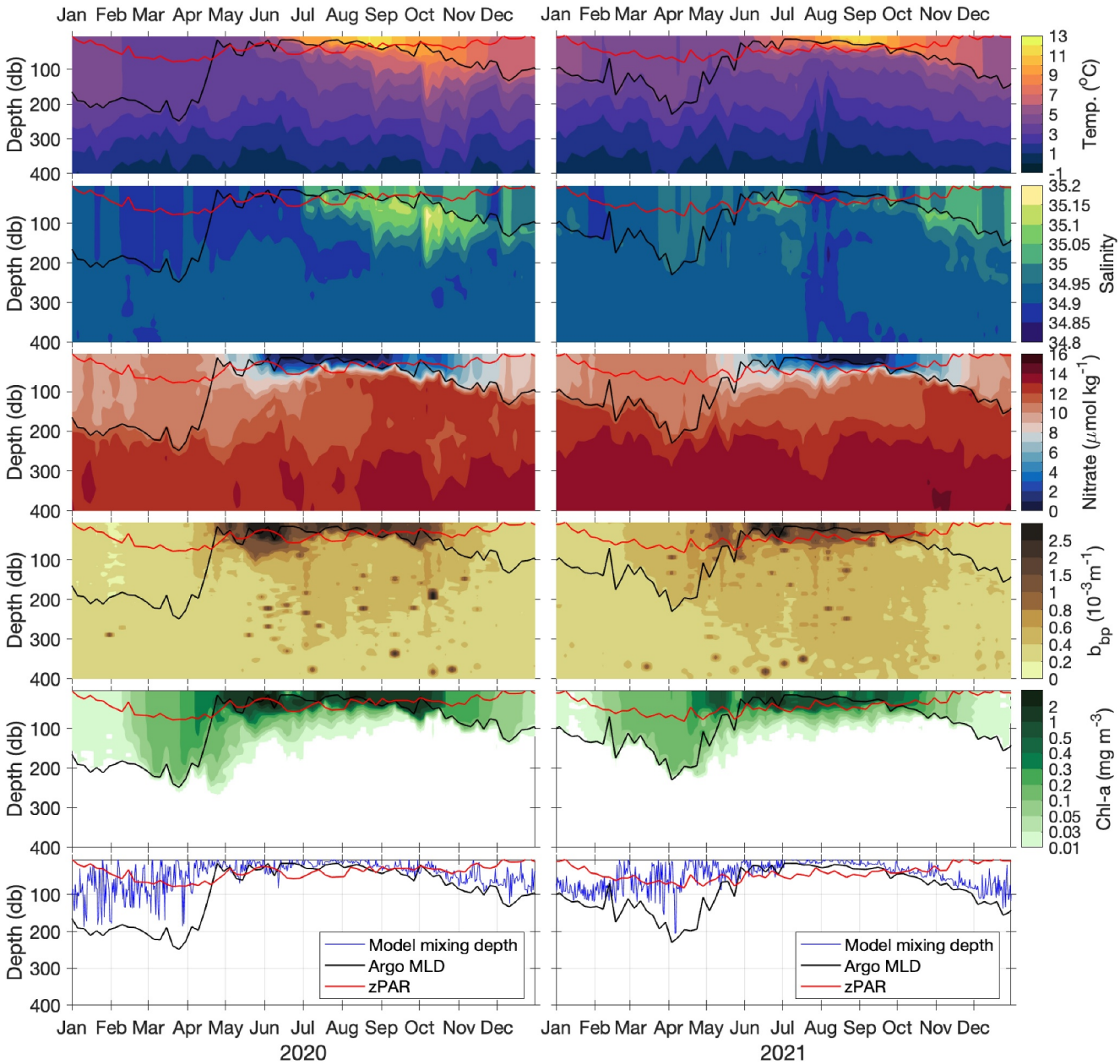

Figure 2. Time series of temperature, salinity, nitrate, backscatter (b_{bp}), and Chl-*a* in the upper 400 m from the Argo floats and mixing depth every 15 hr from the model for 2020 (left hand panels) and 2021 (right hand panels). The mixed layer depth is shown as black or white solid line, while zPAR is shown as a red line. Note that the ranges for b_{bp} and Chl-*a* are non-linear. The minimum value (0.01 mg m^{-3}) for Chl-*a* corresponds to the sensitivity of the fluorescence sensor given by the manufacturer (Table 2).

years and ranged from 25 to 55 m during June–September. The MLD is a product of the history of active mixing, and we observed that maximum modeled mixing depths followed in general the MLDs (Figure 2). The modeled mixing depth was however somewhat shallower than the observed MLD during winter-spring in 2020.

Figure 3 shows the time series of the depth-integrated Chl-*a* (iChl-*a*) and POC (iPOC) over two depth intervals in 2020 and 2021. The depth interval 0–300 m was chosen to include all detectable Chl-*a* in the water column at given point in time. We observed an increase in iChl-*a* at the beginning of February for both 2020 and 2021 (Figures 3a and 3b). During February–March, most of this increase occurred within 0–300 m and not within the shallower depth range (0–42 m). In 2020 iChl-*a* peaked around May–June with additional smaller peaks in mid-July, August, and September–October. In 2021, iChl-*a* developed differently over time as the largest peak was

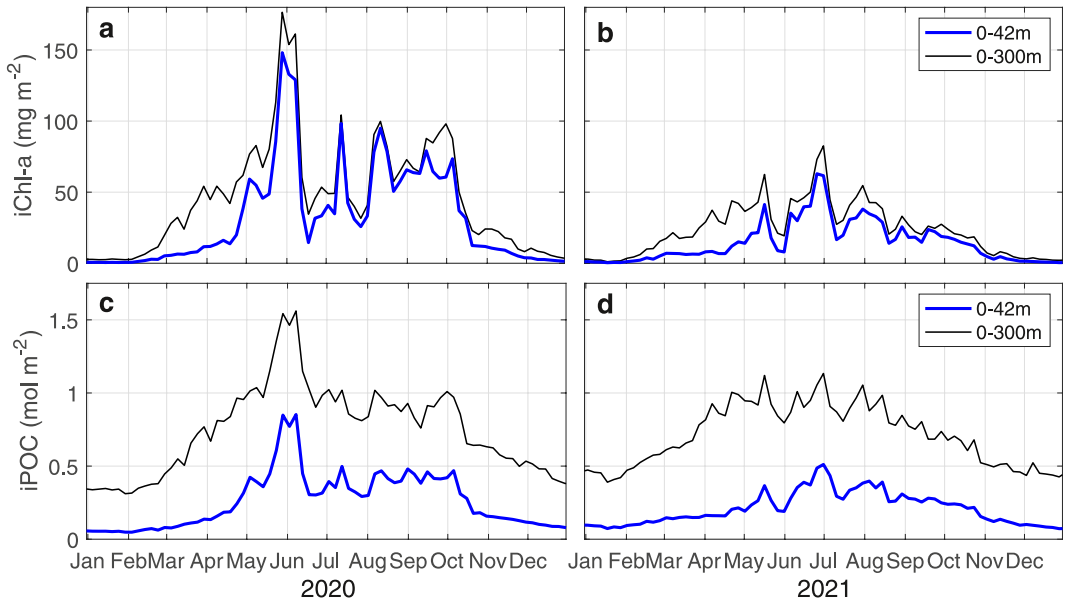

Figure 3. Depth-integrated Chl-*a* (iChl-*a*) (a, b) and particulate organic carbon (iPOC) (c, d) over two depth intervals for 2020 (a, c) and 2021 (b, d).

only half of that in 2020 and appeared about one month later, in June–July. The iPOC time series appeared similar to the iChl-*a* development. In 2020, a large peak in iPOC at both depth intervals also appeared in May–June. In 2021, a smaller peak appeared in June–July at 0–42 m depth.

In both years, average nitrate concentrations in the 0–300 m depth interval, were 11–12 μmol kg^{-1} during winter and about 10 μmol kg^{-1} during summer (Figure 4). Nitrate concentrations at 0–300 m interval were in general slightly higher in 2021 than in 2020. Nitrate at 0–42 m appeared to be utilized much faster in 2020 than in 2021. In 2020, most of the nitrate was depleted in surface waters within one month and by the end of May (equaled to

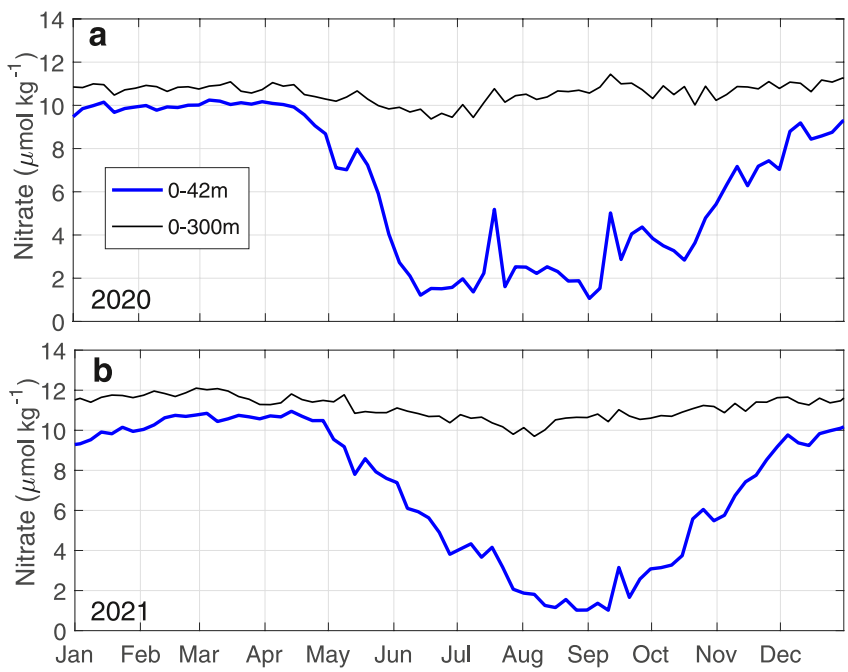

Figure 4. Average nitrate concentrations measured in 2020 (a) and 2021 (b) at two different depth intervals.

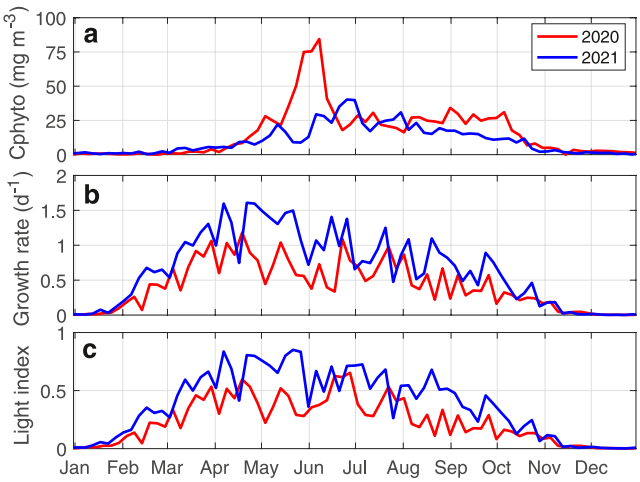

Figure 5. Depth averaged (0–42 m) of phytoplankton carbon (C_{phyto}) (a), phytoplankton growth rate (μ) (b) and light index (I_{light}) (c).

0.2–0.4 μmol kg^{-1} d^{-1}), while it took three months in 2021 to reach similar concentration level by August (0.1 μmol kg^{-1} d^{-1}). The minor increase in surface nitrate concentrations in July 2020, was also observed as a minor, secondary peak in the iChl-*a* (Figure 3a) that co-occurred with a brief ocean heat loss (data not shown) and vertical mixing introducing nutrient-rich deep water into surface waters. From September on surface nitrate concentrations increased again, due to low biological activity and increased mixing with deeper nitrate rich waters, and approached winter values by December.

Time series of estimated phytoplankton carbon biomass (Figure 5a) appeared similar to observed averaged Chl-*a* and POC concentrations. A major peak in C_{phyto} was observed in May–June 2020 and several smaller, less distinct peaks in 2021. Estimated growth rate in both years started to increase in mid-January and dropped to zero again in mid-November (Figure 5b). The growth rates in 2021 were largely higher than in 2020 (Figure 5b), this was also seen in the levels of incident light (Figure 5c). Maximum growth rates peaked in April and June of 2020 (1.1 d^{-1}) and in April–May of 2021 (1.6 $days^{-1}$).

3.2. Seasonal Variability of NPP and NCP

The seasonal, depth integrated NPP and NCP, determined from nitrate profiles for 2020 and 2021, are shown in Figure 6. NPP started to increase in February–March and the largest peak appeared in May–June of 2020 and in mid-June of 2021. The two peaks were of similar magnitude and close to 130 mmol C m^{-2} d^{-1}. In 2021, NPP stopped increasing temporarily in May, decreased until May–June when Chl-*a* was at a local minimum, and then it peaked again in mid-June. Both years had local but smaller peaks in July followed by a gradual and steady decrease until November when zero NPP was reached.

Minor, positive values of NCP were observed in the second half of January 2020 and in February–March of 2021. After that, NCP stayed positive until October 2020 and was only interrupted by shorter periods with negative

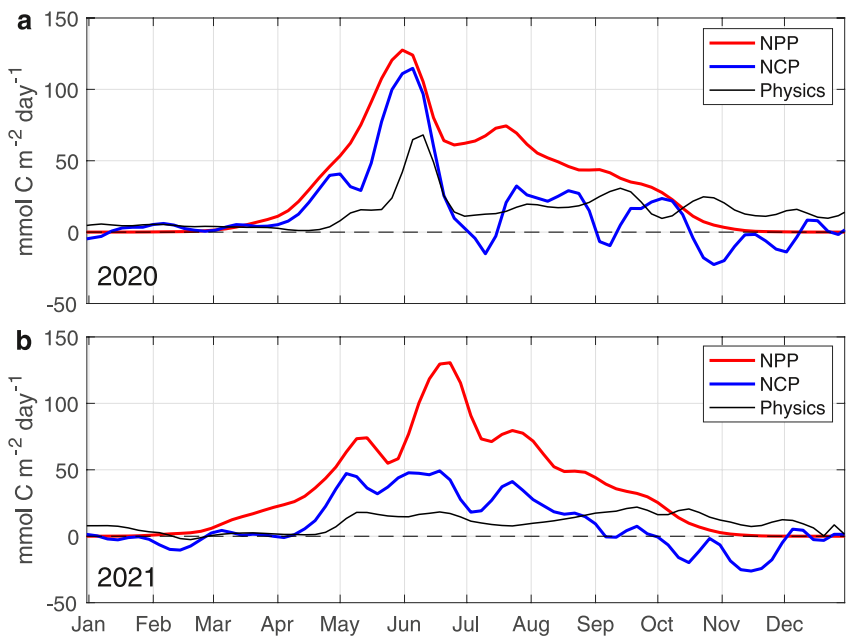

Figure 6. Depth-integrated (0–42 m) rates of net primary production and net community production (NCP) and nitrate rates from physical processes (Equation 9), determined for 2020 (a) and 2021 (b). Positive NCP rates imply nitrate consumption and net production. The nitrate rates from physical processes were converted to carbon using the C:N-ratio of 6.6 (Redfield et al., 1963). The time series were low pass filtered (seven-point Hamming filter).

Table 3
Averaged Annual Depth Integrated (0–42 m) NPP (ANPP), NCP (ANCP), and Heterotrophic Respiration ($R_H \equiv ANPP-ANCP$) for 2020 and 2021

	ANPP	ANCP	R_H
Year		mol C m^{-2} yr^{-1}	
2020	11.7	5.5	6.2
2021	12.4	3.4	9.0

values (Figure 6). In 2020 the June peak in NCP was also reflected as higher Chl-*a* biomass (see Figure 3a), while in 2021 the NCP curve was more leveled. In 2020, the peak in NCP was 120 mmol C m^{-2} d^{-1} while in 2021 maximum NCP was only 50 mmol C m^{-2} d^{-1}. Temporal oscillations seen in the NCP on ∼ monthly scales may derive from variability in physical forcing. for example, during September–November before a deep MLD was developed, the ocean heat loss frequently fluctuated between positive and negative values (data not shown) with associated variability in mixing depth and nutrient mixing. The low pass filter we applied may not completely remove variabilities in the NCP on time scales less than 1 month and smear some of the variability over higher time scales (e.g., ∼monthly scale).

The depth-integrated rates of nitrate introduced to surface water, due to physical processes and estimated by the PWP-model, were either positive or close to zero during both years (Figure 6). Thus, nitrate-rich deep water was continuously brought into surface waters during most of the year. Maximum rates of physical nitrate mixing (70 mmol C m^{-2} d^{-1}) occurred at the beginning of June 2020, immediately after peak levels of nitrate incorporation (NPP and NCP). This was a result of a large vertical gradient in nitrate concentration due to the strong surface nitrate consumption at that time. In 2021, maximum intrusions of nitrate caused by physical processes were lower (about 20 mmol C m^{-2} d^{-1}) and occurred in September.

Even though NCP and phytoplankton biomass started to increase as early as in February–March (2020) and February–April (2021), surface nitrate concentrations did not decrease accordingly during this period (see Figure 4). Intriguingly, a constant or slight increase in surface nitrate concentrations due to nitrate mixing were observed instead (Figure 4). Over this period a rise in Chl-*a* concentrations were noted, by approximately 0.25 mg m^{-3} (equivalent to 10.5 mg m^{-2} over a 42 m depth). By using a regional average C:Chl-a ratio of 61 (Jónasdóttir et al., 2022; Roy et al., 2017) and a C:N ratio of 6.6 (Redfield et al., 1963) this increase in phytoplankton biomass was equivalent to a nitrate utilization of 0.2 μmol kg^{-1}. This marginal change in the nitrate time-series was minor compared to the vertical nitrate flux.

3.3. Annual Averaged NPP and NCP

Annual NPP (ANPP) and annual NCP (ANCP) for 2020 and 2021 were integrated with time, using depth-integrated NPP and NCP for each calendar year. This resulted in an ANPP of 11.7 mol C m^{-2} yr^{-1} and 12.4 mol C m^{-2} yr^{-1}, and an ANCP of 5.5 mol C m^{-2} yr^{-1} and 3.4 mol C m^{-2} yr^{-1} for the years 2020 and 2021, respectively (Table 3). We calculated heterotrophic respiration (R_H) as the difference between ANPP and ANCP. For the two years, 2020 and 2021, heterotrophic respiration was estimated to 6.2 mol C m^{-2} yr^{-1} and 9.0 mol C m^{-2} yr^{-1}, respectively (Table 3). A Kolmogorov–Smirnov hypothesis test (Press et al., 1992) indicated that the ANPP and ANCP were not significant different between the 2 years within a 95% confidence level. The same test assessed, however, that the annual heterotrophic respiration was significantly different between the years (95%, $p = 0.03$).

The principal distinction in the vertical profiles of ANPP and ANCP between the two years was concentrated within the upper ∼25 m, where both ANPP and ANCP were greater in 2020 as opposed to 2021 (Figure 7). At the surface, ANPP was 800 mmol C m^{-3} yr^{-1} in 2020, compared to 580 mmol C m^{-3} yr^{-1} in 2021. In both years ANPP was zero below approximately 60 m depth. Vertical profiles of ANCP below ∼25 m depth for 2020 and 2021 were also comparable (Figure 7) even with a quite different seasonal development of the NCP for the two years (see Figure 6). Maximum ANCP was found at the surface, with nearly twice the rate in 2020 (225 mmol C m^{-3} yr^{-1}) compared to 2021 (120 mmol C m^{-3} yr^{-1}). Both years had positive ANCP (net annual biological production) in the upper 42 m of the water column, and negative ANCP (net annual respiration) between 42 and 175 m depth. Below 175 m, ANCP was close to zero for both years. The highest calculated rates of net community respiration for both years were at 60 m depth, where ANPP also became zero. This occurred primarily in July (2020) and September (2021) (Figure S3 in Supporting Information S1). Deeper than this 60 m threshold, the available light levels were insufficient to support photosynthesis, with net respiration likely being driven by heterotrophic processes. Heterotrophic respiration (R_H) was however, at a maximum at surface in both years.

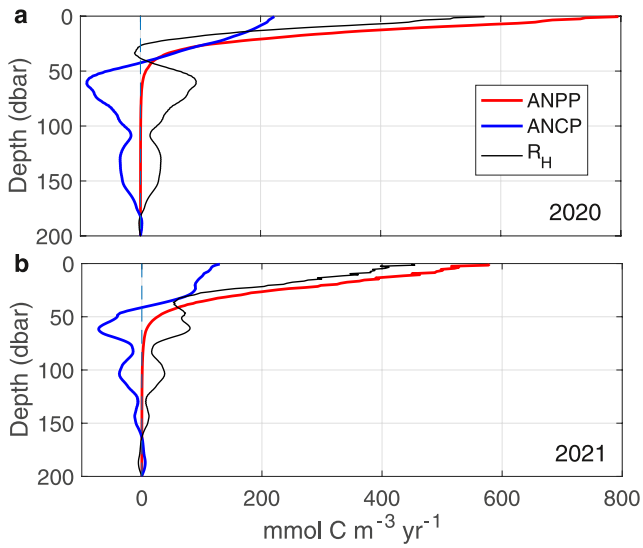

Figure 7. Annual average vertical profiles of ANPP, ANCP and R_H (ANPP-ANCP), for 2020 (a) and 2021 (b).

4. Discussion

Various physical and chemical factors, fluctuating in intensity and duration throughout the year, play a critical role in shaping the extent and success of seasonal phytoplankton growth. Consequently, accurately assessing annual primary production is a complex endeavor, requiring comprehensive seasonal data at high temporal resolution. From Argo BGC-profiling floats, we used 5-day interval depth profiles, to determine NPP and NCP for the Norwegian Sea. In our approach, we utilized a simple one-dimensional physical model to replicate key physical processes. This enabled us to isolate the physically driven nitrate exchange, between the deep-water reservoir and surface waters from the observed nitrate change, that allowed us to calculate annual NCP. When observed nitrate change equaled the modeled nitrate change, NCP becomes zero. This approach is similar to the approach used by Plant et al. (2016) using oxygen and nitrate measurements from the Gulf of Alaska and Briggs et al. (2018) using oxygen and pH measurements in the Southern Ocean. Plant et al. (2016) concluded that oxygen-based estimates of NCP were sensitive to the accuracy of oxygen determinations and that the modeled surface gas exchange needed to be optimized. They therefore concluded that nitrate based ANCP was more reliable than the oxygen based one.

4.1. Seasonal Net Primary and Community Production

As was evident from the Chl-*a* and POC time series (Figure 3), net phytoplankton growth exceeded net respiratory losses at the beginning of February for both years, despite the continued presence of a deep mixed layer. However, due to low numbers and internal variability of the NPP and NCP estimates during this period, precisely pinpointing the beginning of net growth from NPP and NCP can be a challenge. Based on BGC-Argo data from the Norwegian Sea, Mignot et al. (2016) proposed that the onset of the phytoplankton bloom corresponded with a daily photoperiod longer than 10 ± 1 hr. This conclusion was based on observations of weaker and shallower vertical mixing provided a longer photoperiod for phytoplankton, compared to deep mixing events where algal cells are exposed to a shorter photoperiod. Our results showed, however, that when the bloom started the day length was shorter (~7 hr on February 1st). In the PWP-model, from late January (2020) and February (2021) onward, instances of shallow mixing above the minimum light level (z_{PAR}) became more frequent (Figure 2). This occurred even during the presence of a deep winter mixed layer which persisted well into April. This seeming paradox can be attributed to the fact that the deep mixed layer is formed by historical patterns of deep mixing. This observation is similar to the findings of Behrenfeld (2010) who observed North Atlantic phytoplankton bloom events that were initiated during winter when the MLD was at its maximum. Behrenfeld (2010) suggested that deep winter mixing and associated dilution of grazers is essential for bloom formation, as it decouples phytoplankton growth from grazing losses and hence, allowing net growth at sub-optimal light levels.

Physical forcing may explain the striking difference in the seasonal time course of biological incorporation of nitrate and NCP between the 2 years. The observed drop in ocean heat flux in April 2021 (Qnet = −400 Wm^{-2}, Figure 8a) appeared simultaneously with relatively strong winds (20 m s^{-1}, Figure 8b) resulting in an unstable water column and deep mixing (~200 m depth). Therefore, the seasonal MLD needed longer time to shoal than compared to the previous year (Figures 8c and 8d). While the MLD in 2020 shifted from a deep to shallow depth within a month and by the end of April, the shoaling in 2021 was prolonged and a shallow MLD was not reached until May–June. The fast and early shoaling of the MLD in April 2020 initiated a rapid spring bloom. This contrasted with 2021 when a spring bloom peak was absent despite higher growth rate and more favorable light condition compared to 2020. We propose that the reason for this was that deep mixing in April 2021 stirred the phytoplankton within the deep mixed layer and decreased access to photosynthetic light. This slowed down the spring bloom and prolonged the period of nitrate consumption. Consequently, phytoplankton biomass remained at a lower concentration throughout the spring bloom period. The unique combination of lower phytoplankton stocks (C_{phyto} and Chl-*a*), combined with high growth rates in 2021, would imply that grazing pressure and removal of algal biomass was higher than phytoplankton growth in that year. This is also supported by the ~50% higher heterotrophic respiration rates in 2021 than in 2020 (Table 3).

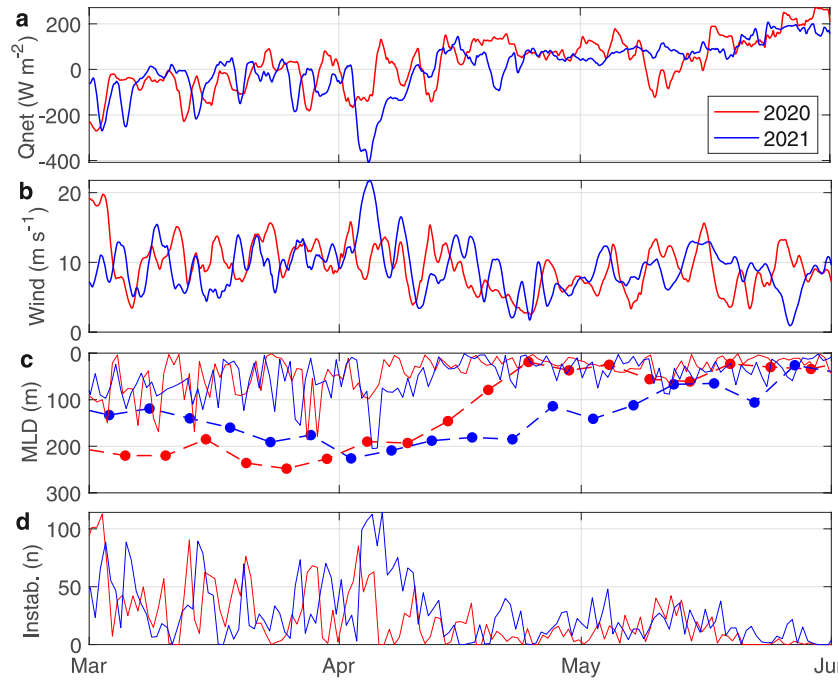

Figure 8. Daily averaged (a) net air-sea heat fluxes (negative values are ocean heat loss), and (b) wind speed for 2020 and 2021 from the ERA5 reanalysis data set, (c) mixed layer depth from Argo floats (dashed lines with filled circles) and mixing depth from model (solid lines), and (d) occurrences of modeled vertical mixing due to static instability. The model data in (c) and (d) are shown every 15 hr. Only data for the periods March–May 2020 (red lines) and 2021 (blue lines) are shown.

Rey (2004) investigated the timing of the spring bloom at Ocean Weather Station M (66°N, 2°E) in the Norwegian Sea, and concluded that late bloom and low phytoplankton biomass probably were associated with stronger grazing pressure. Other studies from the Norwegian Sea have demonstrated the impact by zooplankton grazing on the spring-summer bloom community of phytoplankton (e.g., Bathmann et al., 1990; Wassmann et al., 1991), and grazing pressure can effectively eliminate a bloom as phytoplankton biomass becomes low (e.g., Noji et al., 1996). Børsheim et al. (2014) investigated the phytoplankton bloom in the Nordic Seas using Chl-*a* biomass and estimates of primary production derived from satellite, together with field measurements. They concluded that low Chl-*a* at the end of the spring bloom may have been the result of a succession of highly successful grazers. High Chl-*a* concentrations at the end of the spring bloom period, however, could only occur when phytoplankton outgrew their predators (Børsheim et al., 2014). These studies agree with our observations, and we can conclude that the large discrepancy between NPP and NCP in June–July 2021 was indicative of a larger impact by heterotrophic respiration and zooplankton grazing, initiated by a prolonged, strong ocean heat loss and deep mixing in April 2021.

Grazing pressure in the Norwegian Sea appears to continue after the initial spring bloom event and is only relaxed in autumn when the new zooplankton generations are starting their downward migration prior to the over-wintering period (Melle et al., 2014). Surface nitrate concentrations started to increase again in September, due to deeper mixing caused by stronger wind and strong cooling of surface waters, and the local peak in NCP during September–October 2020 was a direct result of renewed nutrients and less grazing during that time.

4.2. Annual Net Primary and Community Production

Past assessments of ANPP in the Norwegian Sea have revealed significant disparities between estimates derived from satellite data, in-situ measurements, and modeling efforts (Table 4). Skogen et al. (2007) utilized the NORWegian ECOlogical Model system (NORWECOM), a coupled physical, chemical, and biological ocean model, to compute an average ANPP of 6.7 mol C m^{-2} yr^{-1} for the Norwegian Sea. This finding is similar to Rey (2004) who combined multiple, multi-year *in-situ* nitrate profiles to estimate annual primary production in the Norwegian Sea at 80 g C m^{-2} yr^{-1} (corresponding to 6.7 mol C m^{-2} yr^{-1}). The highest estimate however, was derived from satellite data and using the Vertically Generalized Production Model (VGPM, Behrenfeld &

Table 4
Annual NPP and NCP Estimates for the Norwegian Sea

Study	ANPP (mol C m^{-2} yr^{-1})	ANCP (mol C m^{-2} yr^{-1})	Data/method	Integration depth	Area	Period
Falck and Gade (1999)	-	3.0	O_2[a]	30 m	62°N–80°N	1955–1988 (Apr–Sep)
Skjelvan et al. (2001)	-	2.0	O_2[a,b]	300 m	69°N–71°N	1957–1970 and 1991–1998
Skjelvan et al. (2001)	-	2.6	O_2[a,b]	300 m	74°N–75°N	1957–1970 and 1991–1998
Rey (2004)	6.7	-	Nitrate[a]		62°N–73°N	
Falck and Anderson (2005)	-	3.4	Nitrate[a,b]	100 m	62°N–70°N	1981–1988 (Apr-July)
Skogen et al. (2007)	6.7	-	Modeling		62°N–73°N	1981–2004
Børsheim et al. (2014)	14	-	Satellite		63°N–73°N	1998–2012
Possenti et al. (2021)	-	4.2	O_2[c,b]	45 m	63°N–67°N	2014 (Mar–July)
This study	**11.7**	**5.5**	**BGC-Argo**[b]	42 m	**65°N–68°N**	**2020**
This study	**12.4**	**3.4**	**BGC-Argo**[b]	42 m	**65°N–68°N**	**2021**

[a]Estimates are from water samples. [b]vertical flux is included. [c]Sensor data from glider.

Falkowski, 1997), which exceeded all other estimates by more than twofold (Børsheim et al., 2014). Our estimates of the ANPP falls between the lower and higher estimates but is gravitating toward the satellite-derived estimate.

Previous assessments of ANCP shows a range spanning from 2.0 to 4.2 mol C m^{-2} yr^{-1} (Table 4). Estimates derived from O_2 determinations (2.0–3.0 mol C m^{-2} yr^{-1}) appears to be slightly lower than those obtained through alternative methods (3.4–4.2 mol C m^{-2} yr^{-1}). Our estimate of ANCP for 2020 (5.5 mol C m^{-2} yr^{-1}) was higher than previously estimated (Table 4), while the 2021 estimate (3.4 mol C m^{-2} yr^{-1}), was equal to the seasonal estimate based on nitrate-profiles (Falck & Anderson, 2005), confirming the reliability of our findings. Our study used an integrated depth of 42 m, while Possenti et al. (2021) used an integration depth of 45 m as a default choice for calculating the average ANCP, and their estimate lies between our two annual estimates (Table 4). Since our estimates of ANPP for 2020 and 2021 were almost similar, the difference in ANCP between the two years could be explained by higher degree of grazing in 2021 compared to 2020.

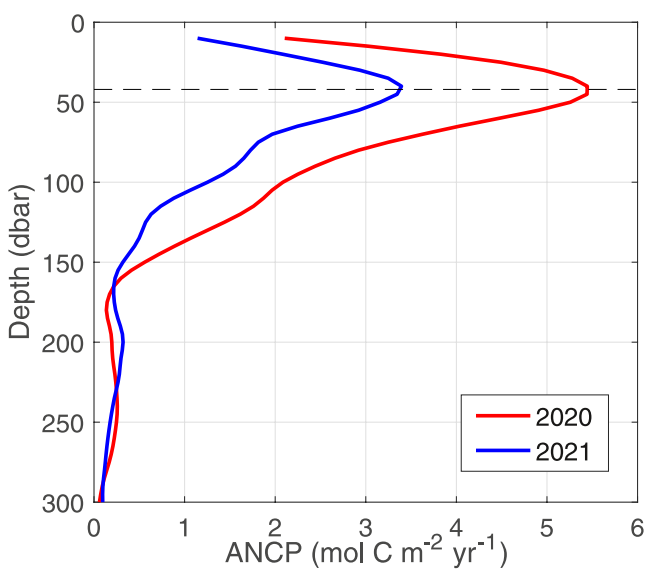

Figure 9. Annual net community production for 2020 and 2021 as function of integration depth. The depth of 42 m is indicated as a dashed line.

Previous ANCP estimates are based on different integration depths, so we estimated the effect of using different depth integrations for ANCP (Figure 9). It follows that by using a depth larger than 42 m, ANCP estimates are getting lower due to an increase in net respiration with depth. For instance, using an integration depth of 100 m would give an ANCP estimate less than half of the estimate at 42 m. Depth integrations down to 175 m would give an ANCP estimate close to zero. Thus, using different integration depths greatly influences the ANCP estimates, and we conclude that cautions should be exercised when comparing ANCP estimates.

Based on this 2-year study, it is evident that disregarding the vertical nitrate flux can result in a considerable underestimation of biological incorporation in surface waters of the Norwegian Sea. To quantify this discrepancy, we evaluated nitrate drawdown in surface waters (0–42 m) during the productive period computed from winter values (March–April) to minimum summer values (medio September) when NCP was positive (see Figure 6). Average nitrate concentrations (0–42 m mean) ranged from approximately 10 μmol kg^{-1} during winter to approximately 1 μmol kg^{-1} during summer for both years. Integrating these seasonal nitrate deficits in the upper 42 m of the water column, and converting them from nitrate to carbon, was equivalent to 2.5 mol C m^{-2} yr^{-1}. By integrating NCP over the same period and depth, we calculated seasonal (April–September) NCP as 5.5 mol C m^{-2} yr^{-1} (2020) and 4.5 mol C m^{-2} yr^{-1} (2021). Thus, nitrate introduced to surface waters

from physical mixing amounted to 3.0 mol C m^{-2} yr^{-1} (2020) and 2.0 mol C m^{-2} yr^{-1} (2021) respectively, constituting 55% (2020) and 44% (2021) of total cellular nitrate-incorporation. This observation is similar to the findings of Falck and Anderson (2005), who also included the vertical nitrate flux in their calculation of new production during the period of April to July. Their calculated vertical upward flux of nitrate into surface waters amounted to 2.5 mol C m^{-2} yr^{-1}, which is similar to our estimate, and corresponded to 74% of their new production estimate (3.4 mol C m^{-2} yr^{-1}). In contrast, Skjelvan et al. (2001) estimated a much lower vertical flux at 0.4 mol C m^{-2} yr^{-1} for the Gimsøy-NW section and 0.2 mol C m^{-2} yr^{-1} for the Bear Island-W section. Similarly, Possenti et al. (2021) found this flux to be negligible. The exact reasons for these disparities are not clear but could potentially be attributed to variations in the integration layer thickness (e.g., 300 m as used by Skjelvan et al., 2001) or by different choice of vertical diffusion coefficient (e.g., 10^{-5} m^2 s^{-1} as used by Possenti et al., 2021).

5. Conclusions

In this study we utilized data from BGC Argo floats to assess phytoplankton bloom dynamics and annual net primary and community production in the Norwegian Sea for the years 2020 and 2021. The distinct growth patterns each year were correlated with hydrographic conditions and physical drivers. To our knowledge this is the first study of annual net primary and community production in the Norwegian Sea based on observations over a full year, allowing us to estimate heterotrophic respiration. The onset of the bloom occurred at the beginning of February each year, coinciding with a deep winter mixed layer. The interplay of physical mechanisms, particularly vertical mixing, exerted significant influence on bloom progression and nitrate consumption in the subsequent months. In April 2021, a notable event with pronounced surface cooling and strong winds led to extensive mixing and a delay in the shoaling of the mixed layer. We propose that this alteration had cascading effects on nitrate utilization, NCP, and respiration (e.g., grazing and removal of phytoplankton biomass). Consequently, this led to a reduction in NCP and appeared to increase the impact by zooplankton grazing and community respiration in 2021 compared to 2020. Across in both years, vertical nitrate mixing from deeper layers to surface emerged as a pivotal factor in determining primary production. Disregarding this mechanism may significantly underestimate biological incorporation of nitrate by a factor of two. These findings underscore the capability of BGC-profiling floats, operating at a 5-day resolution, and their ability to elucidate the intricate interplay between hydrography, physical drivers, and biogeochemical processes in shaping phytoplankton growth dynamics and overall ecosystem productivity in the Norwegian Sea.

Conflict of Interest

The authors declare no conflicts of interest relevant to this study.

Data Availability Statement

The Argo data used in this study were download from an Argo Global Data Assembly (Argo, 2024). Argo float data were collected and made freely available by the International Argo Program and the national programs that contribute to it (https://argo.ucsd.edu, https://www.ocean-ops.org). The Argo Program is part of the Global Ocean Observing System. The code used in the CbPM to compute the NPP is available at https://zenodo.org/record/6599224#23.YqJZFC1h3uM and is presented in Arteaga et al. (2022). The PWP-model used in this study can be found at https://www.cambridge.org/glover (Chapter 15) and has been described in Glover et al. (2011).

Acknowledgments
The Argo data were collected and made freely available by the International Argo Program and the national programs that contribute to it (https://argo.ucsd.edu, https://www.ocean-ops.org). All model codes and data files used in this manuscript are available from the authors upon request. This study was supported by the Institute of Marine Research project "Monitoring of the environment and plankton condition in the Norwegian Sea" and the Research Council of Norway (NorArgo2, #269753). The authors thank the reviewers for constructive comments and suggestions that improved the quality of the manuscript.

References

Argo. (2024). Argo float data and metadata from global data assembly Centre (Argo GDAC) [Dataset]. *SEANOE*. https://doi.org/10.17882/42182

Arteaga, L. A., Behrenfeld, M. J., Boss, E., & Westberry, T. K. (2022). Vertical structure in phytoplankton growth and productivity inferred from biogeochemical-Argo floats and the carbon-based productivity model. *Global Biogeochemical Cycles*, *36*(8), e2022GB007389. https://doi.org/10.1029/2022gb007389

Arteaga, L. A., Boss, E., Behrenfeld, M. J., Westberry, T. K., & Sarmiento, J. L. (2020). Seasonal modulation of phytoplankton biomass in the Southern Ocean. *Nature Communications*, *11*(1), 5364. https://doi.org/10.1038/s41467-020-19157-2

Banse, K. (1991). Rates of phytoplankton cell division in the field and in iron enrichment experiments. *Limnology & Oceanography*, *36*(8), 1886–1898. https://doi.org/10.4319/lo.1991.36.8.1886

Bathmann, U. V., Noji, T. T., & Von Bodungen, B. (1990). Copepod grazing potential in late winter in the Norwegian Sea–a factor in the control of spring phytoplankton growth? *Marine Ecology Progress Series*, *60*, 225–233. https://doi.org/10.3354/meps060225

Behrenfeld, M. J. (2010). Abandoning Sverdrup's critical depth hypothesis on phytoplankton blooms. *Ecology*, *91*(4), 977–989. https://doi.org/10.1890/09-1207.1

Behrenfeld, M. J., Boss, E., Siegel, D. A., & Shea, D. M. (2005). Carbon-based ocean productivity and phytoplankton physiology from space. *Global Biogeochemical Cycles*, *19*(1), GB1006. https://doi.org/10.1029/2004GB002299

Behrenfeld, M. J., & Falkowski, P. G. (1997). Photosynthetic rates derived from satellite-based chlorophyll concentration. *Limnology & Oceanography*, *42*(1), 1–20. https://doi.org/10.4319/lo.1997.42.1.0001

Berger, A. (1978). Long-term variations of daily insolation and quaternary climatic changes. *Journal of the Atmospheric Sciences*, *35*(12), 2362–2367. https://doi.org/10.1175/1520-0469(1978)035<2362:ltvodi>2.0.co;2

Bittig, H. C., Maurer, T. L., Plant, J. N., Schmechtig, C., Wong, A. P., Claustre, H., et al. (2019). A BGC-Argo guide: Planning, deployment, data handling and usage. *Frontiers in Marine Science*, *6*, 502. https://doi.org/10.3389/fmars.2019.00502

Blindheim, J. (1990). Arctic intermediate water in the Norwegian Sea. *Deep-Sea Research, Part A: Oceanographic Research Papers*, *37*(9), 1475–1489. https://doi.org/10.1016/0198-0149(90)90138-I

Børsheim, K. Y., Milutinović, S., & Drinkwater, K. F. (2014). TOC and satellite-sensed chlorophyll and primary production at the Arctic Front in the Nordic Seas. *Journal of Marine Systems*, *139*, 373–382. https://doi.org/10.1016/j.jmarsys.2014.07.012

Boss, E., & Behrenfeld, M. (2010). In situ evaluation of the initiation of the North Atlantic phytoplankton bloom. *Geophysical Research Letters*, *37*(18). https://doi.org/10.1029/2010gl044174

Briggs, E. M., Martz, T. R., Talley, L. D., Mazloff, M. R., & Johnson, K. S. (2018). Physical and biological drivers of biogeochemical tracers within the seasonal sea ice zone of the Southern Ocean from profiling floats. *Journal of Geophysical Research: Oceans*, *123*(2), 746–758. https://doi.org/10.1002/2017jc012846

Brix, H., Gruber, N., Karl, D. M., & Bates, N. R. (2006). On the relationships between primary, net community, and export production in subtropical gyres. *Deep Sea Research Part II: Topical Studies in Oceanography*, *53*(5–7), 698–717. https://doi.org/10.1016/j.dsr2.2006.01.024

Bushinsky, S. M., & Emerson, S. R. (2018). Biological and physical controls on the oxygen cycle in the Kuroshio extension from an array of profiling floats. *Deep Sea Research Part I: Oceanographic Research Papers*, *141*, 51–70. https://doi.org/10.1016/j.dsr.2018.09.005

Dall'Olmo, G., & Mork, K. A. (2014). Carbon export by small particles in the Norwegian Sea. *Geophysical Research Letters*, *41*(8), 2921–2927. https://doi.org/10.1002/2014gl059244

de Boyer Montégut, C., Madec, G., Fischer, A. S., Lazar, A., & Iudicone, D. (2004). Mixed layer depth over the global Ocean: An examination of profile data and a profile-based climatology. *Journal of Geophysical Research*, *109*(C12). https://doi.org/10.1029/2004jc002378

Dugdale, R. C., & Goering, J. J. (1967). Uptake of new and regenerated forms of nitrogen in primary productivity. *Limnology & Oceanography*, *12*(2), 196–206. https://doi.org/10.4319/lo.1967.12.2.0196

Emerson, S. (1987). Seasonal oxygen cycles and biological new production in surface waters of the subarctic Pacific Ocean. *Journal of Geophysical Research*, *92*(C6), 6535–6544. https://doi.org/10.1029/jc092ic06p06535

Falck, E., & Anderson, L. G. (2005). The dynamics of the carbon cycle in the surface water of the Norwegian Sea. *Marine Chemistry*, *94*(1–4), 43–53. https://doi.org/10.1016/j.marchem.2004.08.009

Falck, E., & Gade, H. G. (1999). Net community production and oxygen fluxes in the Nordic Seas based on O_2 budget calculations. *Global Biogeochemical Cycles*, *13*(4), 1117–1126. https://doi.org/10.1029/1999gb900030

Garcia, H. E., Weathers, K., Paver, C. R., Smolyar, I., Boyer, T. P., Locarnini, R. A., et al. (2018). In A. Mishonov Technical (Ed.), *World Ocean Atlas 2018, volume 4: Dissolved inorganic nutrients (phosphate, nitrate and nitrate+nitrite, silicate)* (p. 35). NOAA Atlas NESDIS 84.

Gislefoss, J. S., Nydal, R., Slagstad, D., Sonninen, E., & Holmén, K. (1998). Carbon time series in the Norwegian Sea. *Deep Sea Research Part I: Oceanographic Research Papers*, *45*(2–3), 433–460. https://doi.org/10.1016/s0967-0637(97)00093-9

Glover, D. M., Jenkins, W. J., & Doney, S. C. (2011). *Modeling methods for marine science*. Cambridge University Press.

Graff, J. R., Westberry, T. K., Milligan, A. J., Brown, M. B., Dall'Olmo, G., van Dongen-Vogels, V., et al. (2015). Analytical phytoplankton carbon measurements spanning diverse ecosystems. *Deep Sea Research Part I: Oceanographic Research Papers*, *102*, 16–25. https://doi.org/10.1016/j.dsr.2015.04.006

Helland-Hansen, B., & Nansen, F. (1909). *The Norwegian Sea: Its physical oceanography based upon the Norwegian researches 1900–1904* (p. 390). Bergen: A/S John Griegs Boktrykkeri.

Hersbach, H., Bell, B., Berrisford, P., Hirahara, S., Horányi, A., Muñoz-Sabater, J., et al. (2020). The ERA5 global reanalysis. *Quarterly Journal of the Royal Meteorological Society*, *146*(730), 1999–2049. https://doi.org/10.1002/qj.3803

Holte, J., Talley, L. D., Gilson, J., & Roemmich, D. (2017). An Argo mixed layer climatology and database. *Geophysical Research Letters*, *44*(11), 5618–5626. https://doi.org/10.1002/2017gl073426

Jeansson, E., Olsen, A., & Jutterström, S. (2017). Arctic intermediate water in the Nordic seas, 1991–2009. *Deep Sea Research Part I: Oceanographic Research Papers*, *128*, 82–97. https://doi.org/10.1016/j.dsr.2017.08.013

Johnson, K. S., Plant, J. N., Dunne, J. P., Talley, L. D., & Sarmiento, J. L. (2017). Annual nitrate drawdown observed by SOCCOM profiling floats and the relationship to annual net community production. *Journal of Geophysical Research: Oceans*, *122*(8), 6668–6683. https://doi.org/10.1002/2017jc012839

Jónasdóttir, S. H., Naustvoll, L., Teglhus, F. W., Agersted, M. D., Grenwald, J. C., Melle, W., & Nielsen, T. G. (2022). Calanus finmarchicus basin scale life history traits and role in community carbon turnover during spring. *ICES Journal of Marine Science*, *79*(3), 785–801. https://doi.org/10.1093/icesjms/fsac013

Koestner, D., Stramski, D., & Reynolds, R. A. (2022). A multivariable empirical algorithm for estimating particulate organic carbon concentration in marine environments from optical backscattering and chlorophyll-a measurements. *Frontiers in Marine Science*, *9*, 941950. https://doi.org/10.3389/fmars.2022.941950

Letelier, R. M., Karl, D. M., Abbott, M. R., & Bidigare, R. R. (2004). Light driven seasonal patterns of chlorophyll and nitrate in the lower euphotic zone of the North Pacific subtropical gyre. *Limnology & Oceanography*, *49*(2), 508–519. https://doi.org/10.4319/lo.2004.49.2.0508

Melle, W., Runge, J., Head, E., Plourde, S., Castellani, C., Licandro, P., et al. (2014). The North Atlantic Ocean as habitat for calanus finmarchicus: Environmental factors and life history traits. *Progress in Oceanography*, *129*, 244–284. https://doi.org/10.1016/j.pocean.2014.04.026

Mignot, A., Ferrari, R., & Mork, K. A. (2016). Spring bloom onset in the Nordic seas. *Biogeosciences*, *13*(11), 3485–3502. https://doi.org/10.5194/bg-13-3485-2016

Morel, A., & Maritorena, S. (2001). Bio-optical properties of oceanic waters: A reappraisal. *Journal of Geophysical Research*, *106*(C4), 7163–7180. https://doi.org/10.1029/2000jc000319

Naveira Garabato, A. C., Oliver, K. I., Watson, A. J., & Messias, M. J. (2004). Turbulent diapycnal mixing in the Nordic seas. *Journal of Geophysical Research*, *109*(C12). https://doi.org/10.1029/2004jc002411

Nilsen, J. E. Ø., & Falck, E. (2006). Variations of mixed layer properties in the Norwegian Sea for the period 1948–1999. *Progress in Oceanography*, *70*(1), 58–90. https://doi.org/10.1016/j.pocean.2006.03.014

Noji, T. T., Rey, F., Miller, L., Børsheim, K. Y., Hirche, H. J., & Urban-Rich, J. (1996). Plankton dynamics and sedimentation. In *European subpolar ocean programme: Sea ice-ocean interactions* (Vol. 2, pp. 540–554). Scott Polar Research Institute.

Plant, J. N., Johnson, K. S., Sakamoto, C. M., Jannasch, H. W., Coletti, L. J., Riser, S. C., & Swift, D. D. (2016). Net community production at Ocean Station Papa observed with nitrate and oxygen sensors on profiling floats. *Global Biogeochemical Cycles*, *30*(6), 859–879. https://doi.org/10.1002/2015gb005349

Platt, T., Harrison, W. G., Lewis, M. R., Li, W. K., Sathyendranath, S., Smith, R. E., & Vezina, A. F. (1989). Biological production of the oceans: The case for a consensus. *Marine Ecology Progress Series*, *52*, 77–88. https://doi.org/10.3354/meps052077

Possenti, L., Skjelvan, I., Atamanchuk, D., Tengberg, A., Humphreys, M. P., Loucaides, S., et al. (2021). Norwegian Sea net community production estimated from O_2 and prototype CO_2 OPTODE measurements on a Sea glider. *Ocean Science*, *17*(2), 593–614. https://doi.org/10.5194/os-17-593-2021

Press, W. H., Teukolsky, S. A., Vetterling, W. T., & Flannery, B. P. (1992). *Numerical recipes in C*. Cambridge University Press.

Price, J. F., Weller, R. A., & Pinkel, R. (1986). Diurnal cycling: Observations and models of the upper ocean response to diurnal heating, cooling, and wind mixing. *Journal of Geophysical Research*, *91*(C7), 8411–8427. https://doi.org/10.1029/jc091ic07p08411

Redfield, A. C., Ketchum, B. H., & Richards, F. A. (1963). The influence of organisms on the composition of seawater. *Sea*, *2*(2), 26–77.

Rey, F. (2004). Phytoplankton: The grass of the sea. In H. R. Skjoldal (Ed.), *In the Norwegian Sea ecosystem, 2004* (pp. 97–136). Tapir Academic Press.

Roesler, C., Uitz, J., Claustre, H., Boss, E., Xing, X., Organelli, E., et al. (2017). Recommendations for obtaining unbiased chlorophyll estimates from in situ chlorophyll fluorometers: A global analysis of WET labs ECO sensors. *Limnology and Oceanography: Methods*, *15*(6), 572–585. https://doi.org/10.1002/lom3.10185

Roy, S., Sathyendranath, S., & Platt, T. (2017). Size-partitioned phytoplankton carbon and carbon-to-chlorophyll ratio from ocean colour by an absorption-based bio-optical algorithm. *Remote Sensing of Environment*, *194*, 177–189. https://doi.org/10.1016/j.rse.2017.02.015

Schmechtig, C., Claustre, H., Poteau, A., & D'Ortenzio, F. (2018). BGC-Argo quality control manual for the Chlorophyll-A concentration. https://doi.org/10.13155/35385

Skagseth, Ø., Broms, C., Gundersen, K., Hatun, H., Kristiansen, I., Larsen, K. M. H., et al. (2022). Arctic and Atlantic waters in the Norwegian basin, between year variability and potential ecosystem implications. *Frontiers in Marine Science*, *9*, 831739. https://doi.org/10.3389/fmars.2022.831739

Skjelvan, I., Falck, E., Anderson, L. G., & Rey, F. (2001). Oxygen fluxes in the Norwegian Atlantic current. *Marine Chemistry*, *73*(3–4), 291–303. https://doi.org/10.1016/s0304-4203(00)00112-2

Skjoldal, H. R. (2004). *The Norwegian sea ecosystem* (p. 559). Tapir Academic Press.

Skogen, M. D., Budgell, W. P., & Rey, F. (2007). Interannual variability in Nordic seas primary production. *ICES Journal of Marine Science*, *64*(5), 889–898. https://doi.org/10.1093/icesjms/fsm063

Søiland, H., Prater, M. D., & Rossby, T. (2008). Rigid topographic control of currents in the Nordic seas. *Geophysical Research Letters*, *35*(18), L18607. https://doi.org/10.1029/2008GL034846

Sundby, S., Drinkwater, K. F., & Kjesbu, O. S. (2016). The North Atlantic spring-bloom system—Where the changing climate meets the winter dark. *Frontiers in Marine Science*, *3*, 28. https://doi.org/10.3389/fmars.2016.00028

Voet, G., Quadfasel, D., Mork, K. A., & Søiland, H. (2010). The mid-depth circulation of the Nordic seas derived from profiling float observations. *Tellus A: Dynamic Meteorology and Oceanography*, *62*(4), 516–529. https://doi.org/10.3402/tellusa.v62i4.15697

Wassmann, P. (1990). Relation between primary production and export production in the boreal coastal zone of the Northern Atlantic. *Limnology & Oceanography*, *35*(2), 464–471. https://doi.org/10.4319/lo.1990.35.2.0464

Wassmann, P., Peinert, R., & Smetacek, V. (1991). Patterns of production and sedimentation in the boreal and polar Northeast Atlantic. *Polar Research*, *10*(1), 209–228. https://doi.org/10.1111/j.1751-8369.1991.tb00647.x

Westberry, T., Behrenfeld, M. J., Siegel, D. A., & Boss, E. (2008). Carbon-based primary productivity modeling with vertically resolved photo acclimation. *Global Biogeochemical Cycles*, *22*(2). https://doi.org/10.1029/2007gb003078

Williams, P. J. L. E. B. (1993). On the definition of plankton production terms. *ICES Marine Science Symposia*, *197*(9–19).

Yang, B., Fox, J., Behrenfeld, M. J., Boss, E. S., Haëntjens, N., Halsey, K. H., et al. (2021). In situ estimates of net primary production in the western North Atlantic with Argo profiling floats. *Journal of Geophysical Research: Biogeosciences*, *126*(2), e2020JG006116. https://doi.org/10.1029/2020jg006116